Ionics (2021) 27:1839–1851
https://doi.org/10.1007/s11581-021-03996-0

REVIEW

Using the electron spin resonance to detect the functional centers in materials for sensor devices

Massimiliano D'Arienzo [1] · Franca Morazzoni [1] · Riccardo Ruffo [1] · Roberto Scotti [1]

Received: 29 January 2021 / Revised: 28 February 2021 / Accepted: 1 March 2021 / Published online: 17 March 2021

Abstract

The paper reports and comments the results of several electron spin resonance investigations, performed on semiconductor oxides for gas sensing. The main aspects, related to the comparison between spectroscopic and electric data, are concerning on (i) the role of the oxide defects in interacting with the gas atmosphere; (ii) the origin of the sensing enhancement, which follows the doping of the oxide by transition metal ions; and (iii) the effects of different particle morphology and of the controlled particle shape on the sensing functionality. The electron spin resonance results have been associated, when possible, to those deriving from X-ray photoelectron spectroscopy, in order to investigate the electronic configuration of the transition metal centers. Special emphasis has been deserved to the oxide synthesis procedures, in several cases well related to the electrical response. The data have been drawn from several studies, performed in different time periods, and have been compared to suggest a possible common interpretation of the sensing mechanism, based on either electronic or morphological properties.

Keywords Sensor devices · SnO_2 · ZnO · WO_3 · Electron spin resonance

Introduction

Semiconductor metal oxides are election materials for gas sensor devices. Their sensing ability is connected to variations of the oxide electric properties (resistance) due to interaction of the surface with oxidizing or reducing gases, and it is associated to the increase or decrease in the number of conduction electrons. If the gas interaction causes a reduction, the electrical conductivity increases while, in case of oxidation, the conductivity decreases [1–3]. Among semiconductor metal oxides, the most frequently in use for gas sensing applications are ZnO, SnO_2, and WO_3, owing to their optimal performance and excellent chemical and thermal stability. Over the decades, enormous endeavors have been devoted to enhancing their sensing capability and selectivity, such as by doping with transition metal centers and novel-morphology design of oxide nanostructures [4–6]. Special emphasis has been deserved to study the generation and the location of lattice defects, which appeared to play an important role in tuning the sensing properties [7].

The very essential question, however, remains how to get insights into the fundamental processes of gas sensing [8], that means to describe the electron pathway from the interacting molecule to the oxide surface center and to connect it with the electrical response. In fact, though the macroscopic evidence of the sensing mechanism in semiconductor oxides has been studied for a long time, the electron transfer among the centers responsible for the electrical response remains quite elusive. By deeply investigating the electronic state of these active centers, it is expected that the sensing mechanism should be elucidated at molecular level [9, 10].

One of the most efficient techniques to study the properties of either the electrons located in the semiconductor energy gap or those in the valence band is the electron spin resonance (ESR) [11]. Skipping the fundamentals of this technique, it allows to study the paramagnetic centers under the same experimental conditions as the electrical measurements, which means to detect the properties *quasi in operando*.

As for the experimental ESR parameters, their meaning is here reminded, before the use in the paper. The *g* parameter is a tensor associated either to valence unpaired electrons or to

This paper is dedicated to the late Professor Claudio Maria Mari, who inspired and contributed to the research here reported

✉ Franca Morazzoni
franca.morazzoni@unimib.it

[1] Department of Materials Science, University of Milano-Bicocca, Via Cozzi 55, 20125 Milano, Italy

unpaired electrons in the semiconductor energy gap, and it depends on the energy level trend of the paramagnetic centers.

In the case of the valence electrons:

$$g_{ij} = g_e - 2\zeta \sum_{n \neq \psi_0} \frac{< \psi_0 | L_i | \psi_n >< \psi_n | L_j | \psi_0 >}{E_n^0 - E_0^0}$$

In the case of the gap electrons:

$$g_{ij} = g_e - 2\zeta \sum_{n \neq \psi_0} \frac{< \psi_0 | L_i | \psi_n >< \psi_n | L_j | \psi_0 >}{E_n^0 - E_0^0}$$

If the energy level E_0 is near the conduction band (C_B): $g < g_e$

If E_0 it is near the valence band (VB): $g > g_e$

The above expressions indicate that g_e, i.e., the g value of the free electron value, is modified by the contribution of the spin-orbit coupling interaction (ζ) and of the electron angular momentum interaction (L), both weighted for the energy differences among the ***n*** electronic states interacting with the ground state. Thus, the g tensor value becomes representative of the electronic configuration of the paramagnetic center in the case of valence electrons and can be also associated to the crystal field effects around it **[**12**].** Defect electrons can be associated to their location in the gap.

In the following, a few cases will be described where the contribution of the ESR was determinant to associate the electronic structure of the oxide centers with the sensing mechanism. In some cases, also X-ray-photoelectron spectroscopy (XPS) was effective in indicating the electronic state of transition metal ions**.** The overall results allow to associate the sensing activity to several types of metal centers, as well as to lattice oxygen vacancies, leading to a more rational design of the sensor materials.

The case of functional defects in ZnO semiconductor oxide

The semiconducting properties of ZnO have been investigated for a long time **[**13**]**. A marked variation of the number of electrons in the conduction band has been brought about by modifying the surrounding atmosphere. This behavior was relevant for the use of ZnO as chemical sensor. ZnO belongs to the non-stoichiometric oxide family, due to its excess of metal. The shallow defects, interstitial zinc atoms Zn_i^X or oxygen vacancies V_O^X, act as donor centers as their electrons have sufficient thermal energy to enter the conduction band (respectively $Zn_i^\bullet$ and $V_O^\bullet$ in Scheme 1) **[**14, 15**]**. Temperature and vacuum are able to change the ZnO stoichiometry, thus modifying the pristine defects. Chemisorption of oxidizing or reducing gases at the oxide surface further induces defect modification as the chemisorbed molecules alter the electron amount in the conduction band. Thus, a direct identification of the defects and of their reactivity towards different gases is a fundamental requirement to understand the sensing mechanism at the solid-gas interface and to design the application of this oxide in sensor devices.

Any variation in the amount of interstitial $Zn_i^X/Zn_i^\bullet$ and oxygen vacancies $V_O^X/V_O^\bullet$ generates changes in the material conductivity. Due to the paramagnetic electronic status of ionized zinc defects $Zn_i^\bullet$ and ionized oxygen vacancies $V_O^\bullet$, electron spin resonance is the election technique to identify them. Spectra recorded on ZnO under an inert atmosphere show two groups of signals **(**Fig. 1**) [**16**]**: the first one with g values g_A = 1.955 and g_B = 1.958 and the second one with g_C values at 2.008 and 2.002. Signal A cannot be observed by recording at room temperature, while it becomes very intense at 123 K. Thermal treatments under vacuum lead to an increase of signal B, while A decreases. These results suggest that the signal A is attributable to singly ionized zinc centers, $Zn_i^\bullet$, whose spin-orbit coupling contribution requires the lowering of the temperature at 123 K to detect the signal. The signal B is attributable to ionized oxygen vacancies $V_O^\bullet$; in fact, its intensity increases with the temperature of thermal treatment which removes oxygen from the ZnO lattice.

In summary, according to the symbols in Scheme 1, the following reactions for the generation of paramagnetic $Zn_i^\bullet$ and $V_O^\bullet$ defects in ZnO can be suggested [14, 15]:

Interstitials Zn come from the Frenkel reaction:

$$Zn_{Zn} \leftrightarrows Zn_i^X + V_{Zn}^X \quad (1)$$

Their ionization leads to generation of singly ionized $Zn_i^\bullet$:

$$Zn_i^X \leftrightarrows Zn_i^\bullet + e' \quad (2)$$

Instead, from the Schottky reaction neutral oxygen vacancies arise,

$$Zn_{Zn} + O_O \leftrightarrows V_{Zn}^X + V_O^X + ZnO \quad (3)$$

whose further ionization results in the formation of $V_O^\bullet$ species:

$$V_O^X \leftrightarrows V_O^\bullet + e' \quad (4)$$

Reactions 2 and 4 can be interdependent; this means that the electrons produced by (4) may hinder reaction (2), causing the decrease of the signal A, in agreement with the experimental ESR observations **[**16**].**

While the annealing process in vacuo induces variations of the relative intensities of signals A and B, the successive interaction with oxygen atmosphere enhances the resonance C (Fig. 2), and the formation of the Zn^{++}-O_2^- species has been suggested, based on the values of the g tensor components. The values indicate indeed the presence of two Zn^{++}-O_2^- species, slightly different in the electronic charge of Zn^{++} and

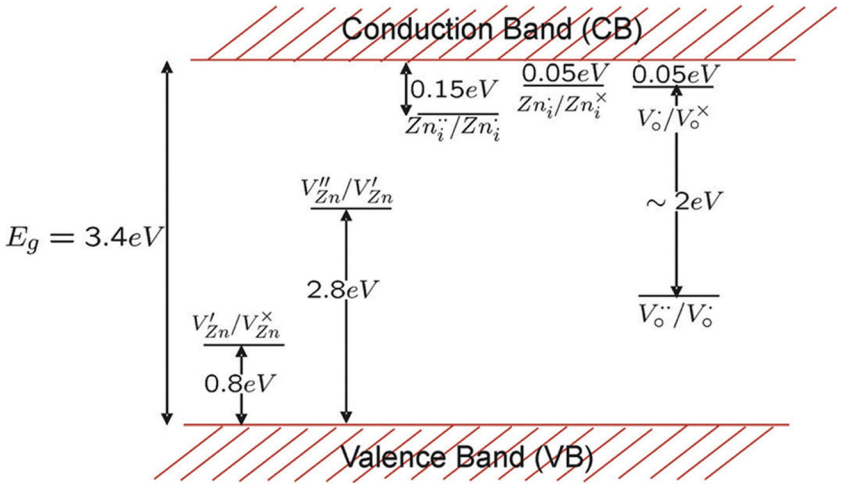

Scheme 1 Energy levels of defects in the energy gap of ZnO [14, 15]

with g-tensor values: g_{1c}[I] = 2.051; g_{1c}[II] = 2.049; g_{2c} [I-II] = 2.008; and g_{3c}[I-II] = 2.002 [17, 18]. At high treatment temperatures, the ionized oxygen vacancies B are the predominant ZnO defects, suggesting that they are mainly involved in

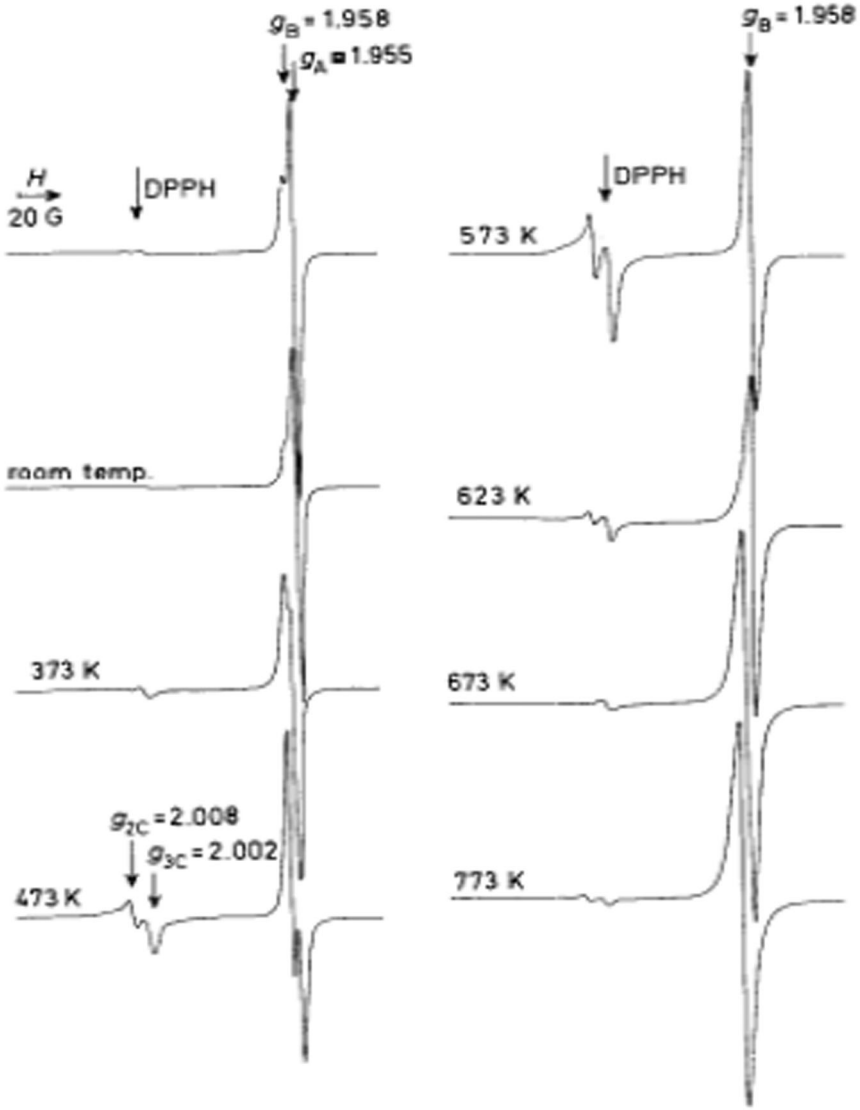

Fig. 1 ESR spectra of the pristine ZnO and of ZnO vacuum thermally treated at various temperatures. The signals C are attributable to the perpendicular component of a rhombic species (see later in the text). Spectra are recorded at 123 K under argon atmosphere [16]

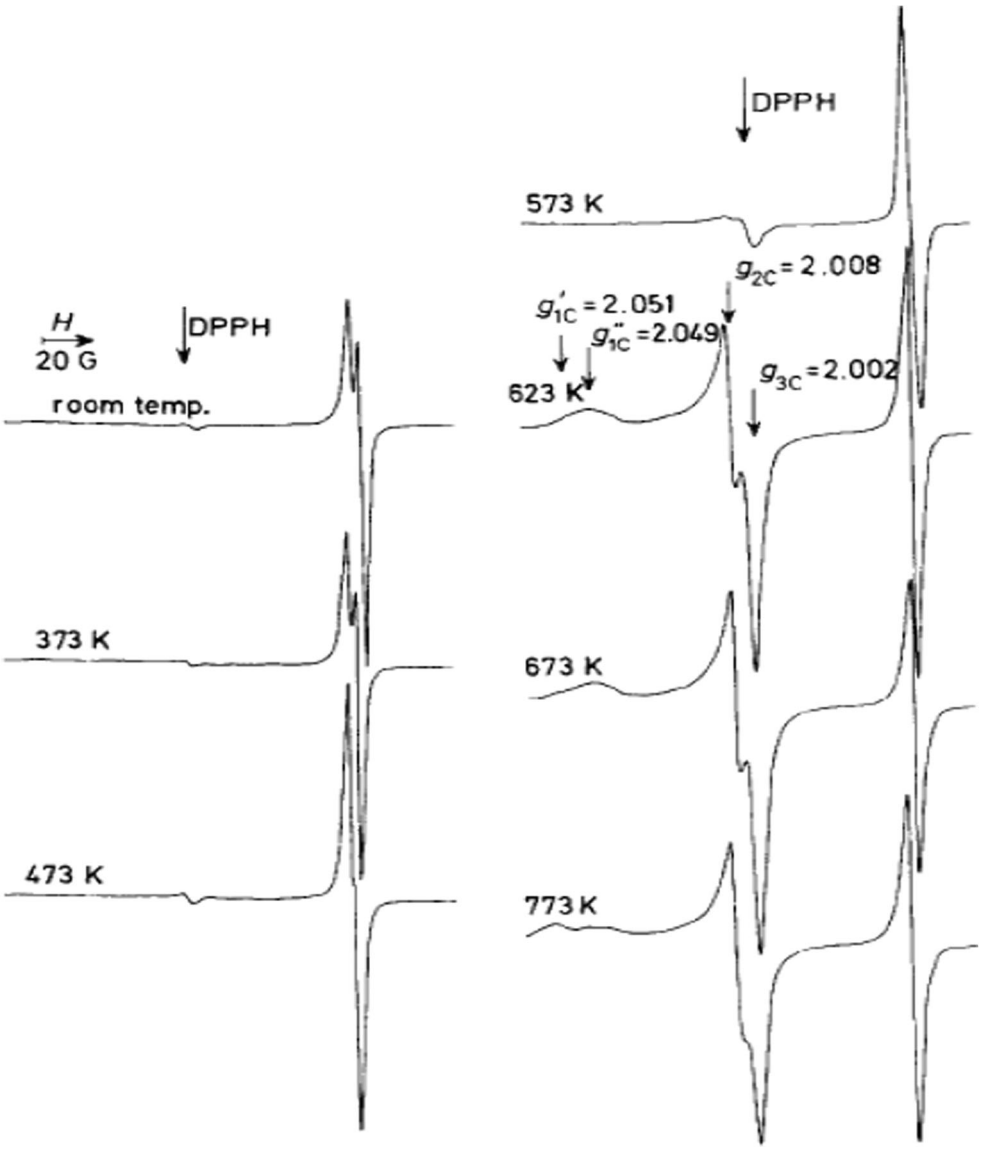

Fig. 2 Variation of the ESR spectrum of ZnO treated in vacuo at the indicated temperature, then contacted with oxygen. Together with the B species $V_O^{\bullet}$ at g = 1.958, two slightly different C species, Zn^{2+}-O_2^-, are well visible [16]

the conductivity change depending on the reducing/oxidative atmosphere. It appears that the electrons trapped into the oxygen vacancies after the annealing under inert atmosphere migrate in the presence of oxygen and give rise to O_2^-; this process causes the decrease of the conductivity (Figs. 2 and 3).

Though most of the interpretations of the ESR spectra reported in the literature have suggested the presence of $Zn_i^{\bullet}$ and $V_O^{\bullet}$ as active defects, a recent insight [19] into the nature of ZnO defects, given by S. Stankic et al., reports a different assignment. This is not the first time that ZnO defects undergo contradictory assignments [20, 21]. In the case of the Stankic work, the author agrees with the former assignment of signal A to $Zn_i^{\bullet}$ species, while the attribution of the defects formed by the in vacuo annealing appears different. In effect, the signal at g = 2.002 observed by Stankic et al. after vacuum annealing has been attributed to $V_O^{\bullet}$ centers. Compared to our results, this proposal is not able to justify the decrease of signals A and B, by contacting the samples annealed in argon with O_2, and the consequent formation of Zn^{++}-O_2^- species (Figs. 2 and 3). Moreover, a g tensor value higher than 2 does not match with an energy level E_0 of the vacancies localized near the conduction band (C_B) of the semiconductor, which instead should have $g < g_e$.

ZnO doped with transition metal ions was also tested in the interaction with oxidizing and reducing gases to study the effect of the metal on the oxo-reductive processes related to the gas sensing. Specifically, ruthenium dispersed on ZnO, studied by ESR [16], showed that the doped oxide, after annealing under an inert atmosphere at 473 K, contains a well detectable amount of oxygen vacancies $V_O^{\bullet}$, Fig. 4 line (a). After contact with O_2, Fig. 4 line (b), $V_O^{\bullet}$ lines disappeared and the resonance lines of Ru^{n+} ($n = 1,3$) at g = 2.12 and of $Ru^{(n+1)}$-O_2^- at $g_{||} = 2.07$ $g_{\perp} = 2.008$ [c] become visible. This suggests that O_2 interacts with $Ru^{(n+1)}$, and very probably O_2

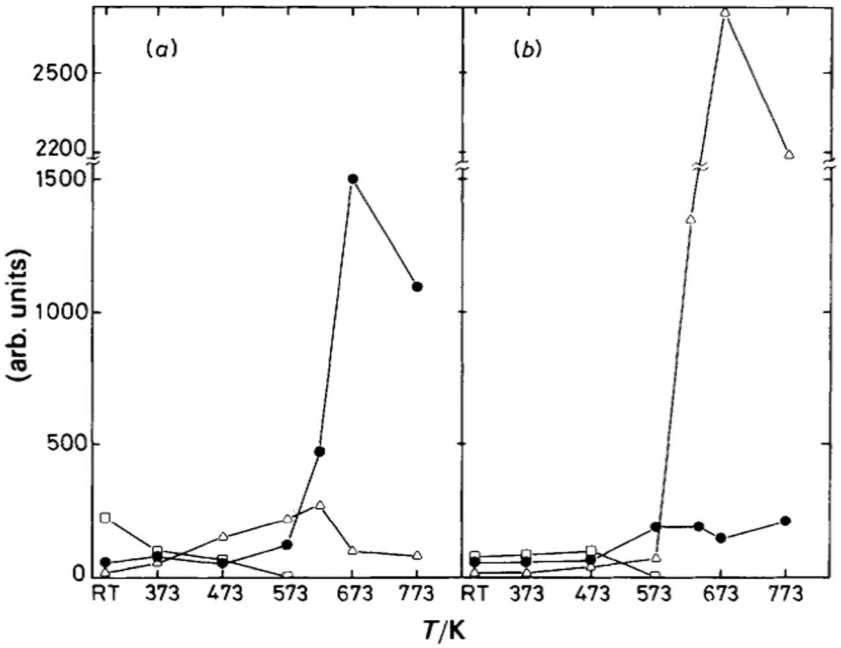

Fig. 3 Variation in the relative amounts of the paramagnetic specie, with the temperature of vacuum treatment: (**a**) ZnO and (**b**) ZnO after O_2 contact: □ species A; ● species B; Δ species C [16]. The relative amount of the paramagnetic centers was determined by deconvolution and double integration of the area of the resonance lines, taking as reference the area of the Varian weak pitch signal (1.0×10^{13} spin cm^{-1}). Accuracy on double integration was ±15%

receives electrons from the metal center, while $V_O^{\bullet}$ defects are no more visible.

More recently, due to the increased ability in preparing various nanostructures, ZnO has been modified either in the morphology or in the chemical composition (by doping with several transition metals) to improve the electric response and to implement its use in sensing devices at lower temperature. Ref. [22] reviewed these material modifications and suggest a possible origin of the activation mechanism given by metals. Nevertheless, the mechanism there reported appears a bit incomplete (see Scheme 2). It proposes the location of superoxide anion O_2^- on the ZnO surface (Scheme 2b), while it did not mention the pathway of the electrons moving from the semiconductor to reduce O_2 and causing the depletion layer. The noble metal is then indicated as responsible for the enlargement of the depletion layer (Scheme 2c), but still no electron pathway was indicated.

It seems to us a suitable suggestion to formulate a pathway of the electrons during the interaction of the sensor material with the surrounding atmosphere. The transition metal should receive electrons from the oxygen vacancies enlarging the depletion layer (reaction 6); after that, the molecular oxygen firstly interacts with the transition metal center, thus lowering its reduction potential, and then receives electrons from the transition metal. This is really what appears from our ESR data [16].

$$V_O^X \leftrightarrows V_O^{\bullet} + e' \quad (5)$$

$$M^{m+} + n\,V_O^{\cdot} \leftrightarrows M^{(m-n)+} + n\,V_O^{\cdot\cdot} \quad (6)$$

$$M^{(m-n)+} + n\,O_{2(g)} \leftrightarrows M^{n+} + nO_2' \quad (7)$$

Thus, the additional depletion region correctly reported in Scheme 2c seems to us an electron accumulation due to

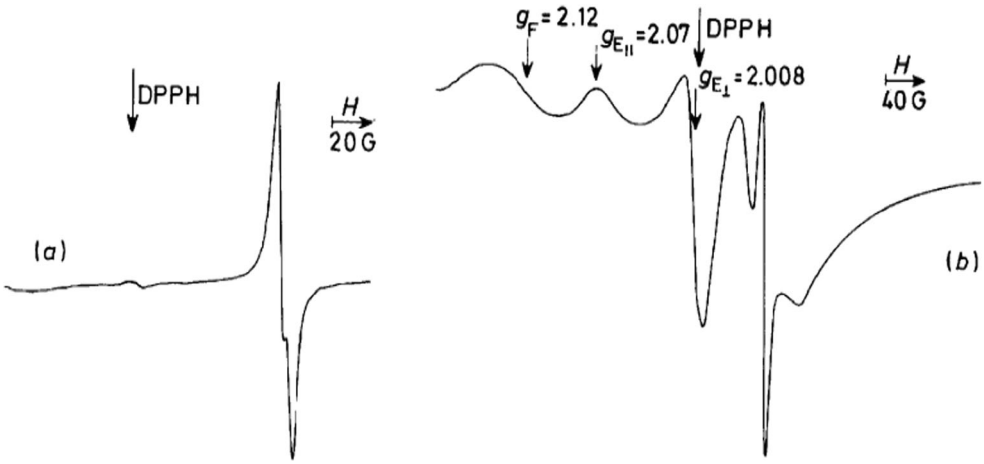

Fig. 4 ESR spectra recorded at 123 K of (**a**) Ru-doped ZnO annealed at 473 K in argon (**b**) the same after contact with O_2 [16]

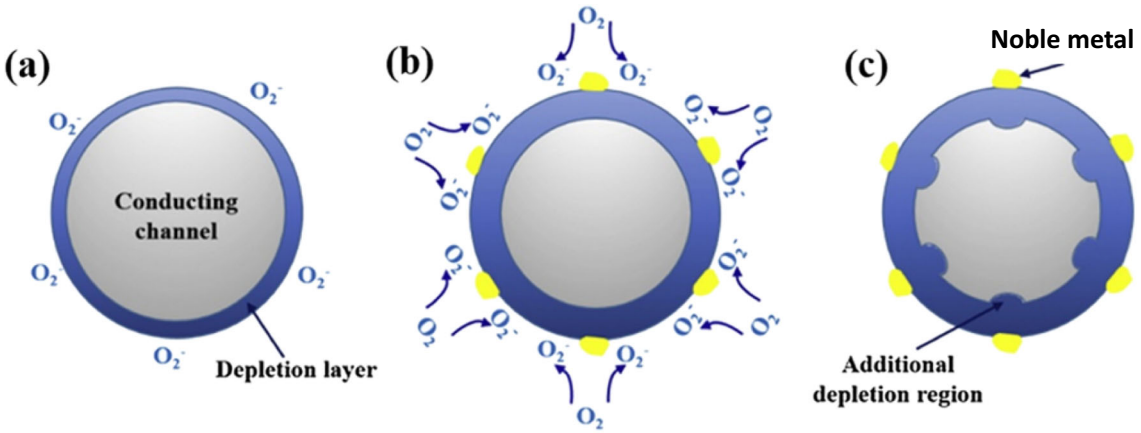

Scheme 2 Schematic representation of the oxygen interaction with noble metal-doped semiconductor [22]

reaction (6), which increases the depletion region and enhances the electrical response.

The relevance of the ESR studies on ZnO here reported consists in using a spectromagnetic investigation, in general associated to molecular centers, for describing the electronic state of the centers, also defective, in ionic materials and for indicating the dynamic of the semiconductor electrons under different atmospheres.

The case of functional defects in SnO_2 semiconductor oxide: chemical and morphological features

Chemical features

SnO_2 is nowadays one of the most common commercial materials used in gas sensor devices. Although it was synthesized in very different morphologies to obtain better electrical response [23], its improvement in electrical response and selectivity still passes through a better knowledge of the sensing mechanism at micro/nano level. The scientific aim of the reported ESR studies was to assess which species are responsible for the SnO_2 conductivity, both in pristine materials with different morphologies and in the chemically modified oxide. In the following, the interactions with carbon monoxide of pristine and metal-doped SnO_2 will be described. The sensing properties of SnO_2 can be generally enhanced by the chemical doping with transition metal ions [24], this becoming a key point in the research about the gas sensing applications. In all the reported cases, the samples were prepared by sol-gel procedure which allows the direct comparison between ESR and electric data, due to the high homogeneous and reproducible composition obtained with this technique.

SnO_2 and Pt-doped SnO_2 prepared as a thin film were treated by reducing (CO/argon) and oxidizing (air) atmospheres. The ESR spectra show significant differences (Fig. 5) [25–27].

In pure SnO_2 film treated with CO, the resonance line at $g = 1.890$ attributable to ionized oxygen vacancies ($V_O^{\bullet}$) is clearly evident (Fig. 5a) while in Pt-doped SnO_2, treated under the same conditions, no $V_O^{\bullet}$ are detectable. Upon contact with air, the species Sn^{4+}-O_2^-, having $g_1 = 2.023$ $g_2 = 2.005$ $g_3 = 1.999$, becomes evident in Pt-doped SnO_2 film (Fig. 5b). Conversely, in pure SnO_2 film, superoxide species are almost undetectable, and the amount of $V_O^{\bullet}$ centers apparently does not change [25–27]. This behavior is slightly different in SnO_2 powders where, after reaction with reducing gases CO [25–27 and references therein] or NO [28], the amount of oxygen vacancies decreases and that of superoxide species increases.

Based on these results, the following processes have been suggested:

For pure SnO_2

$$CO + O_O \leftrightarrows V_O^X + CO_2 \qquad V_O^X \leftrightarrows V_O^{\bullet} + e' \tag{8}$$

where O_O is an oxide anion in a regular lattice site.

For Pt-doped SnO_2

$$Pt^{4+} + nV_O^{\cdot} \leftrightarrows Pt^{(4-n)+} + n\,V_O^{\cdot\cdot} \tag{9}$$

$$Pt^{(4-n)+} + n\,O_{2(g)} \leftrightarrows Pt^{4+} + nO_2' \tag{10}$$

$$nSn^{4+} + n\,O_2^- \leftrightarrows nSn^{4+}{-}O_2' \tag{11}$$

The overall reaction interpretation was that all the electrons which in pure SnO_2 are constrained into subsurface oxygen vacancies by the potential barrier at the film-gas interface, in Pt-doped SnO_2 migrate to Pt^{4+}surface centers, due to the favorable difference in the Fermi level. Hence, they are transferred to oxygen and give Sn^{4+}-O_2^-. It appears that the Pt ions act as an electron sink enlarging the depletion layer zone. The

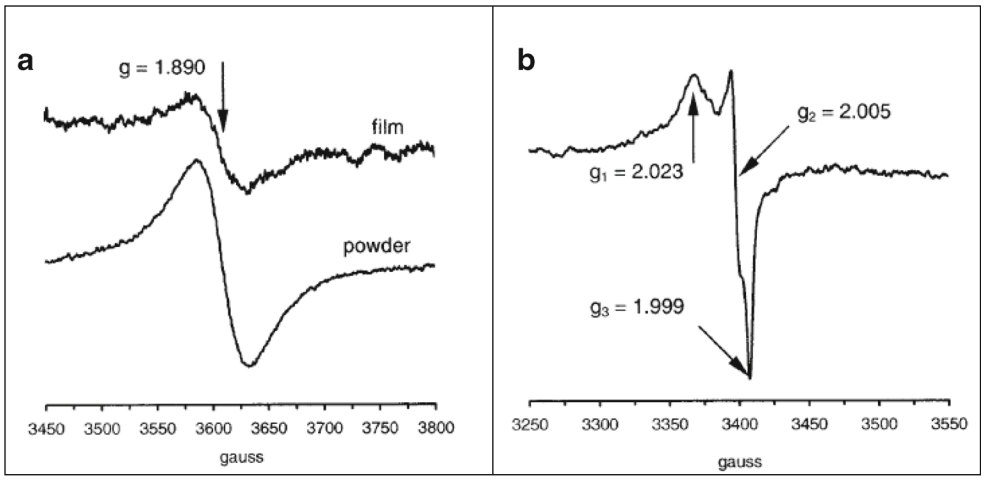

Fig. 5 EPR signals of (**a**) $V_O^{\bullet}$ in SnO_2 powder and films treated with CO (600 ppm)/Ar at 673 K (1 atm under static conditions) and (**b**) Sn^{4+}-O_2 in Pt-doped SnO_2 films treated in CO (600 ppm)/Ar stream at 673 K (50 cm^3 min^{-1}) and successively in air stream at 298 K (50 cm^3 min^{-1}) [25–27]

electrons are thus transferred from the vacancies to the oxygen, enhancing the electrical response (Fig. 6), which has been reported in terms of ratio between the resistance in air over the resistance in the different atmosphere. The ratio better highlights variations higher than 1 order of magnitude (values of 5,10, and 50 corresponds to the 80%, the 90%, and the 95% of the air resistance variation). Significantly, $V_O^{\bullet}$ on pristine SnO_2 film is not able to transfer electrons to O_2, probably due to a subsurface location, while Pt centers, which received the electrons from the vacancies, are responsible for the response in air.

A direct proof of the electrons pathway is the reduction of Pt^{4+} towards less positive values, as observed by X-ray photoelectron spectroscopy (XPS) in samples treated by CO (Fig. 7).

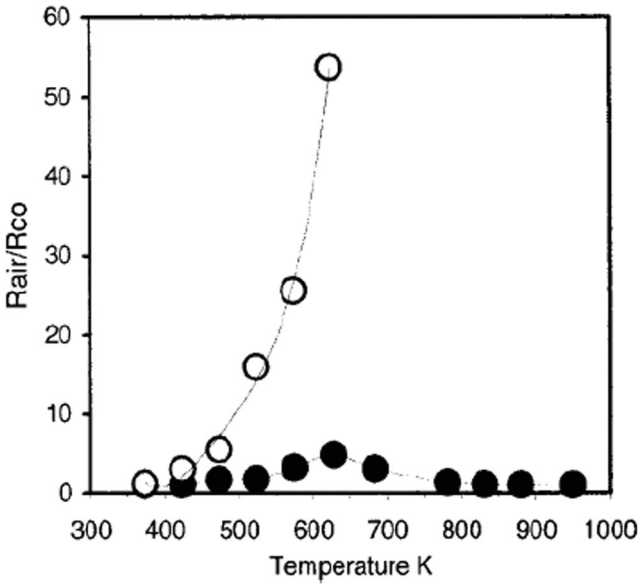

Fig. 6 Plot of electrical response (R_{air} = electrical resistance in dry air; R_{CO} = electrical resistance in 800 ppm of CO in dry air) vs temperature for Pt-doped SnO_2 films. Open circles annealed at 673 K, full at 973 K. The dot size represents the measurement error [25–27]

In the literature, no further convincing suggestions based on ESR studies are reported which propose a possible electron pathway from the SnO_2 oxygen vacancies to the molecular oxygen, through the transition metal center. A recent paper of Grishina et al. [29] attributed to oxygen vacancies some resonances of SnO_2, even if with energy in contrast with the literature data; besides, in spite of a correct identification of the transition metal ion centers, no relationship with the sensor functionality has been suggested. More intriguing are the reports of Kolmakov [30], who proposed two operative sensing mechanisms for SnO_2 and the related Pd-doped oxide: the electronic mechanism and the chemical mechanism. The electronic mechanism hypothesizes that some large depletion zones form around the metal particles in the presence of O_2 (Fig. 8b), and this causes variation in the electron flow (see arrows in Fig. 8a).

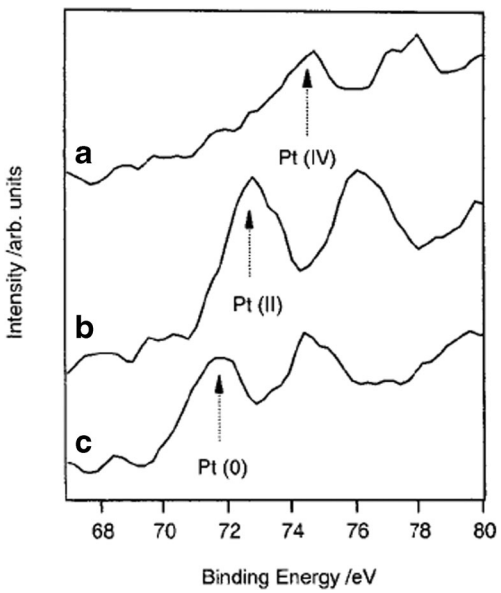

Fig. 7 XPS spectrum of the Pt4f region in Pt-doped SnO_2 film. (**a**) Annealed in air; (**b**) treated with CO at 373 K; and (**c**) treated with CO at 673 K [25–27]

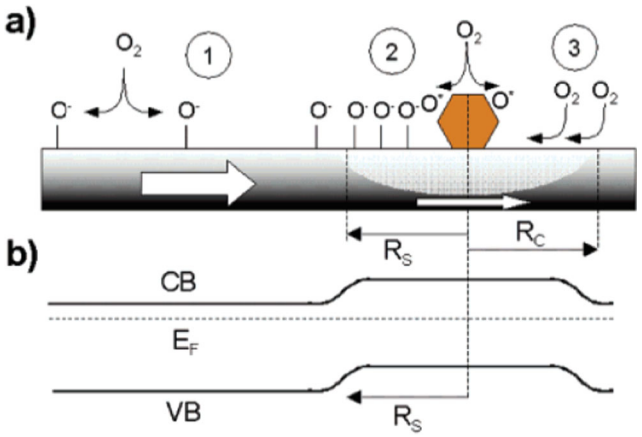

Fig. 8 Processes on SnO_2 and transition metal-doped nanowires. (1) Ionosorption of oxygen at defect sites on pristine SnO_2 (2) molecular oxygen dissociation on transition metal nanoparticles (3) capture by transition metal nanoparticle of weakly adsorbed O_2 diffused along the tin surface. R_s is the spillover radius; R_c is the radius of the collection zone [30]

The chemical mechanism suggests that the oxygen molecules diffuse through the semiconductor surface (back spillover effect) and reach the transition metal, where their dissociation is catalyzed by the metal particle (Fig. 8a). The O^- spilling should increase the rate of repopulation of the oxygen vacancies and the rate of the SnO_2 electrical response towards oxygen. As in the case of ZnO, our evidences, which are mainly based on the ESR data, demonstrated that the oxygen vacancies can transfer electrons to the transition metal centers (see the below reported case of inverted opal SnO_2); O_2 molecules receive electrons from the transition metal center stabilizing the Sn^{4+}-O_2^-species. The major differences with Kolmakov lie in the dissociative chemisorption of oxygen to give O^- species he proposed and in the lack of any hypotheses for the electronic changes of the oxygen vacancies and of the metal centers. Our suggestion hypothesizes that the interaction of O_2 with Pt centers becomes active and lowers the reduction potential of the metal cation, allowing oxygen reduction. The behavior we described for platinum can be associated to palladium and ruthenium under reducing and oxidizing atmosphere [31].

$$Pt^{4+} + nV_O^{\cdot} \leftrightarrows Pt^{(4-n)+} + n\,V_O^{\cdot\cdot} \quad (12)$$

$$Pt^{(4-n)+} + nO_{2(g)} \leftrightarrows Pt^{4+} + nO_2^{\prime} \quad (13)$$

The hypotheses we have formulated regarding the pathway of the electrons from the vacancies to the oxygen and suggested as molecular source of the electrical response were commented by A. Gurlo [32]. This author outlines that the experiments on semiconductor oxides have been carried out in atmosphere conditions different from the real operative ones (e.g., CO in air). It is true, however, that the necessity of revealing the species obliged us to fully separate the study under oxidizing atmospheres from that under the reducing one. In mixed atmospheres, the species cannot be easily distinguished.

Morphological features: the inverted opals

The semiconductor chemical composition is not the only responsible for the SnO_2 electrical response. During the past years, several ceramics were prepared with the form of ordered architectures of high surface area opal and inverted opal. Among them, SnO_2 inverted opal, a material built by nanocrystalline bridges and junctions around a regular arrangement of air spheres, should in principle display stronger gas response, due to the large surface area and the interconnection between holes (Fig. 9) [33].

The interaction of CO with either pure and Ru(Pt)-doped SnO_2 has been investigated to understand the morphology-function relationship and to compare the electric response of the inverted opal samples with that of the nanostructured thin films. It resulted that, under CO contact, the transition metal centers in inverted opal samples decrease their oxidation state (Ru^{4+} becomes Ru^{3+} ESR active) following the already suggested process:

$$Ru(Pt)^{4+} + n\,V_O^{\cdot} \leftrightarrows Ru\,(Pt)^{(4-n)+} + nV_O^{\cdot\cdot} \quad (14)$$

Figure 10a reports the $V_O^{\bullet}$ centers for differently annealed inverted opal SnO_2 and Fig. 10b the Ru^{3+} centers due to CO interaction. By contact with oxygen, no O_2^- is formed. A possible hypothesis is that the reduction of oxygen to oxide proceeds very fast to repair the surface damaged by CO and rebuilds the original surface.

The electrical response is not quantitatively different from that of nanopowdered materials, while it is faster and more reproducible (Fig. 11). The reproducibility may be attributed to the regular shape of the surface and of the hierarchical structure always retained.

Morphological features: shape-controlled nanoparticles

The results on the inverted opals sensor materials suggested that the control of the morphology, not just of the particle size (nanosized particles), is able to guarantee a better reproducibility of the electrical response. In fact, several studies have recently outlined that engineering of the crystal facets in metal oxides provides tailored electrical response and selectivity in gas sensing, due to the unique properties and defectivity associated to different atom arrangements, bond energies, and charge densities. In particular, for SnO_2 nanocrystals having different abundance of {221}, {111}, and {110} surfaces, the differences in the sensing ability were attributed both to the higher surface energy of the {221} and {111} compared to the {110} faces and to the presence on these surfaces of undercoordinated cations, i.e., five- and four-fold coordinated Sn^{4+}, which seem to foster the chemisorption of ionized oxygen species, promoting the reactivity with the reducing gas

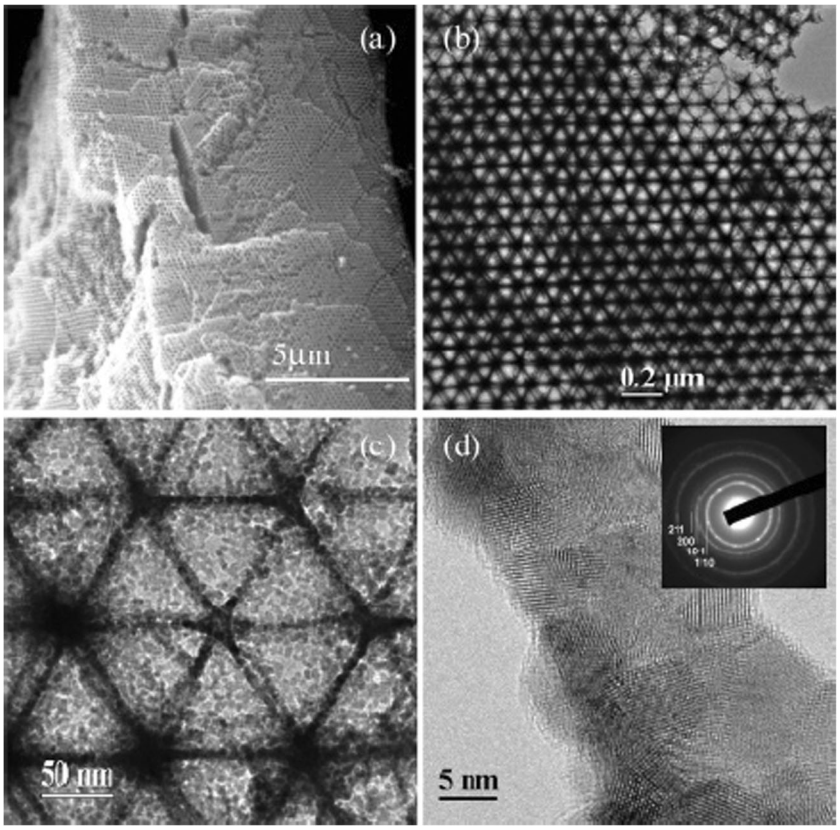

Fig. 9 (**a**) SEM micrographs, (**b**–**c**) TEM, and (**d**) HRTEM images of Ru-doped SnO_2 inverted opal. In the inset, the indexes of SnO_2 crystal structure are indicated [33]

[34–38]. This hypothesis was based exclusively on the Yamazoe mechanism [39, 40], attributing the conductivity variations to the surface chemisorption and removal of oxygen ions, without considering the role of oxygen vacancies, whose nature and concentration are greatly dependent on the morphological and surface features of the nanomaterials [41, 42].

In this context, we have prepared shape-controlled octahedral (OCT), elongated dodecahedral (DOD), and nanobar (NBA) SnO_2 nanocrystals enclosing well defined types of exposed crystal surfaces and studied their interaction with carbon monoxide by tracking the generation and reactivity of oxygen defects with ESR [43], trying to shed light on the role of the exposed crystal faces in the sensing mechanism. Figure 12 associates the different behavior of nanoparticles, demonstrating that a strong relation exists among particle shape, oxygen vacancies (g = 1.89) produced by CO

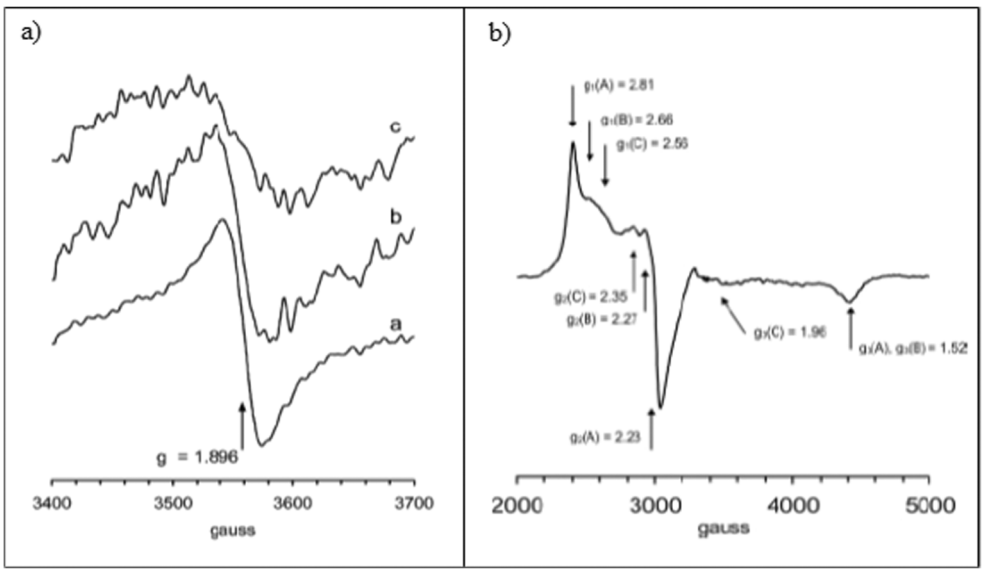

Fig. 10 ESR spectra of (**a**) inverted opal SnO_2 annealed at increasing temperature from a to c and (**b**) Ru^{3+} centers [33]

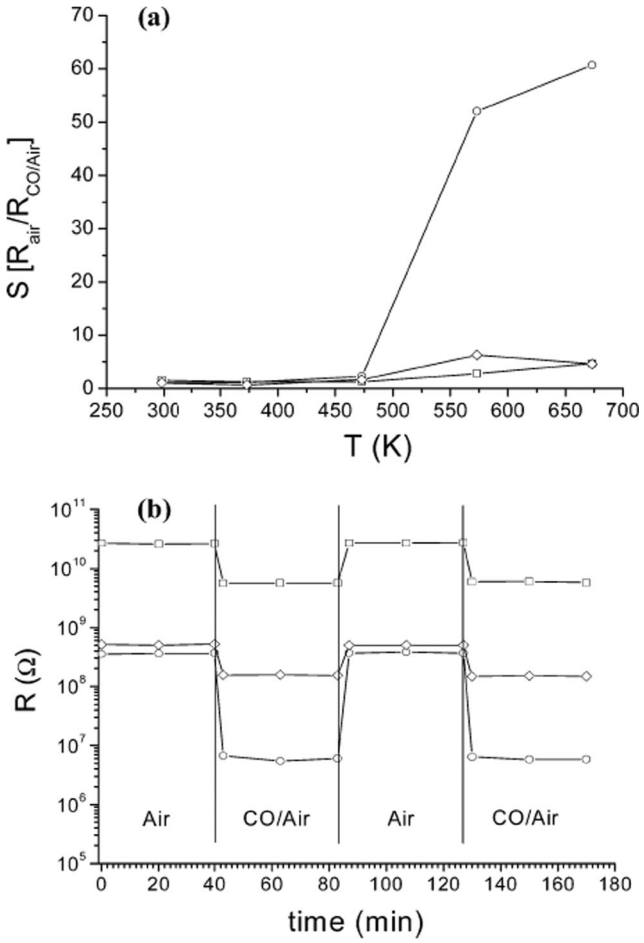

Fig. 11 **a** Plot of the electrical response (R_{air} = electrical resistance in dry air; R_{CO} = electrical resistance in 800 ppm of CO in dry air) vs T(K) for (□) SnO_2 (◊) Ru-doped SnO_2 (○) Pt-doped SnO_2. **b** Resistance variation under two subsequent pulses alternating air to CO/air mixture. Symbols are the same as in (**a**). The dot size represents the measurement error [33]

interaction, and the electrical response. Thus, it appears that the structure of the faces in the different shape particles determines the different sensing activity, and the mechanism is still mediated by the oxygen defects V_O^+. The responsibility of forming a great number of oxygen vacancies lies in the abundance of exposed {221} and {111} faces (respectively in OCT and DOD species). Unexpectedly, the reaction with air, after CO interaction, does not lead to the formation of Sn^{4+}- O_2^-. As in the case of inverted opal SnO_2, it could be suggested that the reduction of molecular oxygen proceeds very fast to repair the surface damage induced by CO interaction, re-constructing the pristine particle surface. The relation among exposed facet, oxygen vacancies, and electrical response in Fig. 12 is very impressive and confirms the key role of the oxygen vacancies in modulating the sensing mechanism.

In summary, tailoring the gas sensing properties by morphology control represents a promising research field. Various SnO_2 nanostructures with tuneable porosity, size, and exposed surfaces were successfully synthesized in recent years, revealing that the relative concentration of $V_O^\bullet$ defects is morphology-dependent and supporting the idea to exploit the controlled generation of these defects not only for boosting the electrical response but also the selectivity of the sensors [44].

The case of functional defects in WO_3 semiconductor oxide

The use of WO_3 as sensing material is less frequent than that of SnO_2; thus, the behavior of this semiconductor oxide is less investigated. It was found that its electrical response is complementary to SnO_2-based sensors and, interestingly, gives distinguishable responses for the reducing (CO) or the oxidizing (NO_2) gases [45, 46].

A frequent use of WO_3 is to detect ammonia. Under NH_3 contact, the resistance decreases, due to the following reactions, all releasing electrons:

$$2NH_3 + 3O_O \rightarrow N_2 + 3H_2O + 6e^- \quad (15)$$

$$2NH_3 + 4O_O \rightarrow N_2O + 3H_2O + 8e^- \quad (16)$$

$$2NH_3 + 5O_O \rightarrow 2NO + 3H_2O + 10e^- \quad (17)$$

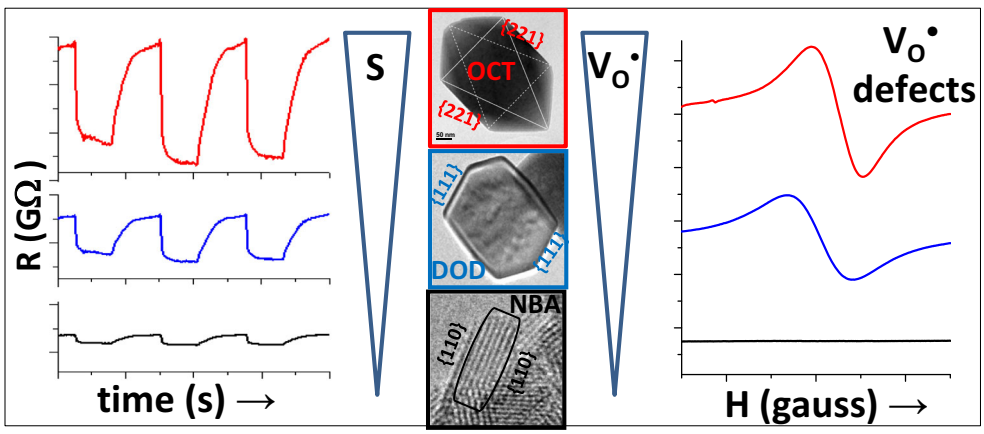

Fig. 12 Comparison between oxygen defect and electrical response for different shaped nanoparticle under CO interaction [43]

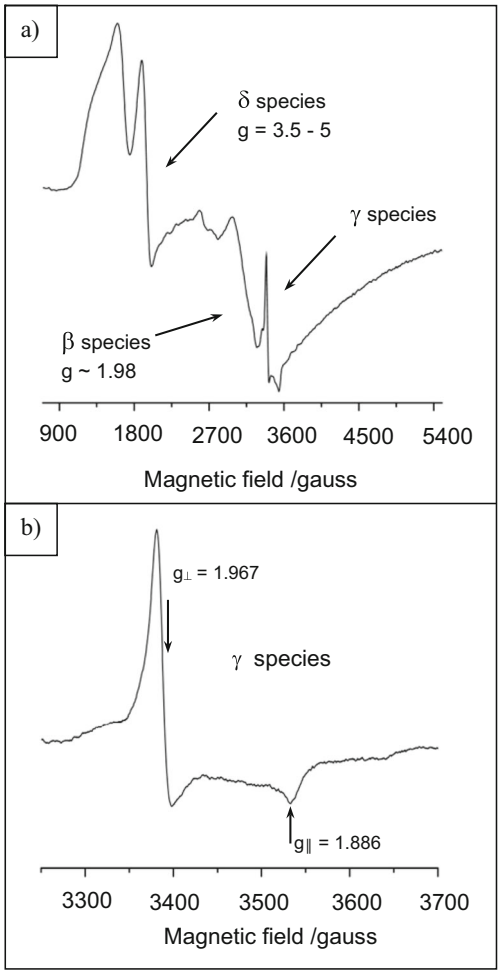

Fig. 13 **a** Cr(III) and **b** Cr(V) species in as-prepared Cr-doped thin films [47]

The electrical response of WO_3 increases by transition metal doping, and the investigation of the transition metal centers becomes once again mandatory to understand the sensing mechanism. Mesoporous sol-gel-derived WO_3 thin films doped with Pt and Cr have been prepared and investigated by ESR spectroscopy [47], in order to give a rational to the electrical response under ammonia contact. Cr(III) and Cr(V) centers are well visible in the ESR spectra of the as-prepared samples, suggesting a good dispersion of this metal in the oxide matrix (Fig. 13). Platinum was instead detected as metal nanoparticles mainly located inside WO_3.

Macroporous WO_3 films with inverted opal structure [48] were also prepared and investigated by X-ray photoelectron spectroscopy. W(VI) centers of WO_3, Cr(III), and Pt(0) centers of the doping metals were clearly detected, confirming the ESR results on sol-gel prepared samples.

In the presence of the transition metal ions, the conduction band electrons are expected to migrate to the metal itself, allowing further electron to be released (reactions 10–12) and enhancing the electrical response. Pt-doped materials, indeed, show better electrical response (Fig. 14).

The reason of the higher catalytic activity in presence of Pt particles is probably that they act as catalysts in the interaction between ammonia and O_O centers, decreasing the activation barrier for the N-H bond dissociation in NH_3. Notably in the present case are the transition metal centers, not the WO_3 defects, to be able to be investigated by ESR. Their behavior however allows only indirect hypotheses, as the ESR spectra have not been taken under sensing atmosphere; it cannot be excluded that under operative conditions, also oxygen vacancies become visible.

Conclusions

Looking at the literature, which proposes the sensing mechanism of the semiconductor oxides, it seems that the major contributions to explain the behavior of these materials come from the morphological and elemental surface analyses, beside of course from the fundamental studies of the electrical properties.

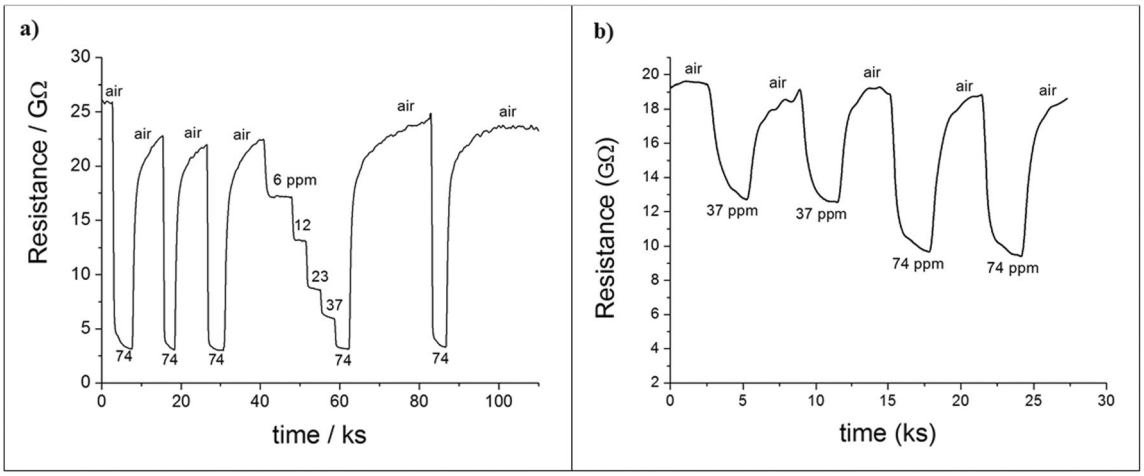

Fig. 14 Electrical resistance of different sensing elements: **a** Pt-doped WO_3 and **b** Cr-doped WO_3 towards the indicated concentration of NH_3 in air [47]

A comprehensive study of the electronic properties of the active centers, especially as concerns on the defects and doping elements most likely triggering the variation of the electrical response, has been rarely reported before and sometimes with controversial interpretations.

ESR represents a very sensitive technique to detect and monitor intrinsic paramagnetic defects or doping centers, which release or accept electrons under different atmospheres, and to formulate a trustable sensing mechanism based on their electronic state. Also, the electron pathway between the oxide and the chemisorbed molecules can be hypothesized and connected to the electrical response**.** The main criticism inherent to the ESR conclusions is that they have not been gained strictly *in operando*. As an example, the spectra of SnO_2-based samples have been recorded on the semiconductor in pure reducing, or alternatively oxidizing atmospheres. Thus, the data indicate what happens under the two extreme conditions and are crucial to indicate the electrons pathway from the reducing to the oxidizing atmosphere. The results give an indication of the mechanism which could not be obtained in *operando*, due to the simultaneous presence of the oxidizing and the reducing atmospheres.

Finally, concerning on the role of the oxygen vacancies already present or thermally formed into the oxide lattice, they behave as trigger agents of the electrical response and change their electronic state depending on the gas interaction; certainly, they act as reservoir of electrons and transfer electrons to the doping metals**.**

Funding Open access funding provided by Università degli Studi di Milano - Bicocca within the CRUI-CARE Agreement.

References

1. Barsan N, Weimar U (2001) Conduction model of metal oxide gas sensors. J Electroceram 7:143–167
2. Barsan N, Hübner M, Weimar U (2013) Conduction mechanism in semiconducting metal oxide sensing films. In: Jaaniso R, Tan OK (eds) Semiconductor gas sensors, 1st edn. Woodhead Publishing Limited, Cambridge, pp 35–63
3. Dey A (2018) Semiconductor metal oxide gas sensors: a review. Mater Sci Eng B 229:206–217
4. Vander Wal RL, Hunter GW, Xu JC, Kulis MJ, Berger GM, Ticich TM (2009) Metal-oxide nanostructure and gas-sensing performance. Sensors Actuators B Chem 138:113–119
5. Rock F, Barsan N, Weimar U (2008) Electronic nose: current status and future trends. Chem Rev 108:705–725
6. Gurlo A (2011) Nanosensors: towards morphological control of gas sensing activity. SnO2, In2O3, ZnO and WO3 case studies. Nanoscale 3:154–165
7. Armelao L, Barreca D, Bontempi E, Canevali C, Depero LE, Mari CM, Ruffo R, Scotti R, Tondello E, Morazzoni F (2002) Can electron paramagnetic resonance measurements predict the electrical sensitivity of SnO2-based film? Appl Magn Reson 22:89–100
8. Ji H, Zeng W, Li Y (2019) Gas sensing mechanisms of metal oxide semiconductors: a focus review. Nanoscale 11:22664–22684
9. Barsan N, Koziej D, Weimar U (2007) Metal oxide-based gas sensor research: how to? Sensors Actuators B Chem 121:18–35
10. Weimar U (2017) Operando Methods. Available: https://weimar.ipc.uni-ingen.de/index.php?id=833
11. Roessler MM, Salvadori E (2018) Principles and applications of EPR spectroscopy in the chemical sciences. Chem Soc Rev 47:2534–2553
12. Morazzoni F (2021) Symmetry in inorganic and coordination compounds, Springer, due April 14 2021
13. Zhu L, Zeng W (2017) Room-temperature gas sensing of ZnO-based gas sensor: a review. Sensors Actuators A Phys 267:242–261
14. Schmidt-Mende LS, MacManus-Driscoll JL (2007) ZnO-nanostructures, defects, and devices. Mater Today 10:40–47
15. Han J, Mantas PQ, Senos AMR (2002) Effect chemistry and electrical characteristics of undoped and Mn-doped ZnO. J Eur Ceram Soc 22:49–59
16. Morazzoni F, Scotti R, Volonté S (1990) Electron paramagnetic resonance investigation of paramagnetic point defects in ZnO and ZnO-supported ruthenium. J Chem Soc Faraday Trans 86:1587–1591
17. Lunsford JH (1974) ESR of adsorbed oxygen species. Catal Rev 8:135–157
18. Cattania Sabbadini MG, Gervasini A, Morazzoni F, Strumolo D (1987) Electron Spin Resonance Investigations of Ruthenium supported on γ-Alumina. J Chem Soc Faraday Trans 83:2271–2277
19. Zhang M, Averseng F, Haque F, Borghetti P, Krafft J, Baptiste B, Cosentin G, Stankic S (2019) Defect-related multicolour emissions in ZnO smoke: from violet, over green to yellow. Nanoscale 11:5102–5115
20. Qu J, Ge Y, Zu B, Li Y, Dou X (2016) Transition-metal-doped p-type ZnO nanoparticle-based sensory array for instant discrimination of explosive vapors. Small 12:1369–1377
21. Ischenko V, Polarz S, Grote D, Stavarache V, Fink K, Driess M (2005) Adv Funct Mater 15:1945–1954
22. Ren Q, Cao Y, Arulraj D, Liu C, Wu D, Wei-Ming L, Ai-Dong L (2020) Resistive-type hydrogen sensors based on zinc oxide nanostructures. J Electrochem Soc 167:067528
23. Li B, Zhou Q, Peng S, Liao Y (2020) Recent advances of SnO2-based sensors for detecting volatile organic compounds. Front Chem 8:321
24. Scotti R, Canevali C, Mattoni M, Morazzoni F, Armelao L, Barreca D (2008) Nanostructured Pt-doped tin oxide films. Mater Synth 117-126
25. Morazzoni F, Canevali C, Chiodini N, Mari CM, Ruffo R, Scotti R, Armelao L, Tondello E, Depero LE, Bontempi E (2001) Nanostructured Pt-doped tin oxide films: sol-gel preparation, spectroscopic and electrical characterization. Chem Mater 13:4355–4361

26. Li Y, Zu B, Guo Y, Li K, Zeng H, Dou X (2016) Surface superoxide complex defects-boosted ultrasensitive ppb-level NO2 gas sensors. Small 12:1420–1424
27. Canevali C, Chiodini N, Di Nola P, Morazzoni F, Scotti R, Bianchi CL (1997) J Mater Chem 7:997–1002
28. Canevali C, Mari CM, Mattoni M, Morazzoni F, Ruffo R, Scotti R, Russo U, Nodari L (2004) Mechanism of sensing NO in argon by nanocrystalline SnO2: electron paramagnetic resonance, Mössbauer and electrical study. Sensors Actuators B Chem 100: 228–235
29. Grishina DA, Mironov AA, Pentegov IS, Marikutsa AV, Konstantinova EA (2012) Electron spin resonance chaacterization of defects in sensor materials based on nanocrystalline tin dioxide. Proc SPIE Int Soc Opt Eng. https://doi.org/10.1117/12.923460
30. Kolmakov A, Klenov DO, Lilach Y, Stemmer S, Moskovits M (2005) Enhanced gas sensing by individual SnO2 nanowires and nanobelts functionalized with Pd catalyst particles. Nano Lett 5: 667–673
31. Canevali C, Mari CM, Mattoni M, Morazzoni F, Nodari L, Ruffo R, Russo U, Scotti R (2005) Interaction of NO with Nanosized Ru-, Pd-, and Pt-doped SnO2: electron paramagnetic resonance, Mossbauer, and electrical investigation. J Phys Chem B 109: 7195–7202
32. Gurlo A (2006) Interplay between O2 and SnO2: oxygen Ionosorption and spectroscopic evidence for adsorbed oxygen. Chem Phys Chem 7:2041–2052
33. Acciarri A, Barberini R, Canevali C, Mattoni M, Mari CM, Morazzoni F, Nodari L, Polizzi S, Ruffo R, Sala M, Scotti R (2005) Ruthenium(platinum) – doped tin dioxide inverted opal for gas sensors: synthesis, electron paramagnetic resonance, Mossbauer and electrical investigation. Chem Mater 17:6167–6171
34. Han X, Jin M, Xie S, Kuang Q, Jiang Z, Jiang Y, Xie Z, Zheng L (2009) Synthesis of tin dioxide octahedral nanoparticles with exposed high-energy {221} facets and enhanced gas-sensing properties. Angew Chem Int Ed 48:9180–9183
35. Zou XX, Li GD, Wang PP, Su J, Zhao J, Zhou LJ, Wang YN, Chen JS (2012) A precursor route to single-crystalline WO3 nanoplates with an uneven surface and enhanced sensing properties. Dalton Trans 41:9773–9780
36. Zheng H, Ou GZ, Strano MS, Kaner RB, Mitchell A, Kalantarzadeh K (2011) Nanostructured tungsten oxide – properties, synthesis, and applications. Adv Funct Mater 21:2175–2196
37. Malik R, Tomer VK, Mishra YK, Lin L (2020) Functional gas sensing nanomaterials: a panoramic view. Appl Phys Rev 7:021301
38. Wang X, Han X, Xie S, Kuang Q, Jiang Y, Zhang S, Mu X, Chen G, Xie Z, Zheng L (2012) Controlled synthesis and enhanced catalytic and gas-sensing properties of tin dioxide nanoparticles with exposed high-energy facets. Chem Eur J 18:2283–2289
39. Huang J, Matsunaga N, Shimanoe K, Yamazoe N, Kunitake T (2005) Nanotubular SnO2 templated by cellulose fibers: synthesis and gas sensing. Chem Mater 17:3513–3518
40. Xu C, Tamaki J, Miura N, Yamazoe N (1991) Grain size effects on gas sensitivity of porous SnO2-based elements. Sensors Actuators B 3:147–155
41. Ji H, Zeng W, Li Y (2019) Gas sensing mechanisms of metal oxide semiconductors: a focus review. Nanoscale 11:22664–22684
42. Hashem MA, Akbar S, Morris P (2019) Role of oxygen vacancies in nanostructured metal-oxide gas sensors: a review. Sensors Actuators B Chem 301:126845
43. D'Arienzo M, Cristofori D, Scotti R, Morazzoni F (2013) New insights into the SnO2 sensing mechanism based on the properties of shape controlled tin oxide nanoparticles. Chem Mater 25:3675–3686
44. Motsoeneng RG, Kortidis I, Ray SS, Motaung DE (2019) Designing SnO2 nanostructure-based sensors with tailored selectivity toward propanol and ethanol vapors. ACS Omega 4:13696–13709 and references therein
45. Dong C, Zhao R, Yao L, Ran Y, Zhang X, Wang Y (2020) A review on WO3 based gas sensors: morphology control and enhanced sensing properties. J Alloys Compd 820:153194
46. Staerz A, Somacescu S, Epifani M, Kida T, Weimar U, Barsan N (2020) WO3 – based gas sensors: identifying inherent qualities and understanding the sensing mechanism. ACS Sens 5:1624–1633
47. D'Arienzo M, Crippa M, Gentile P, Mari CM, Polizzi S, Ruffo R, Scotti R, Wahba L, Morazzoni F (2011) Sol-gel derived mesoporous Pt and Cr-doped WO3 thin films: the role played by mesoporosity and metal doping in enhancing the gas sensing properties. JSol-Gel Sci Technol 60:378–387
48. D'Arienzo M, Armelao L, Mari CM, Polizzi S, Ruffo R, Scotti R, Morazzoni F (2011) Macroporous WO3 thin films active in NH3 sensing: role of the hosted Cr isolated centers and Pt nanoclusters. J Am Chem Soc 133:5296–5304